Research Square

Preprints are preliminary reports that have not undergone peer review.
They should not be considered conclusive, used to inform clinical practice,
or referenced by the media as validated information.

Disentangling the Sources of Spectral Induced Polarization of Microbial Systems: Experiments in Non-Geological Media

Satoshi Izumoto

satoshi.izumoto@hotmail.co.jp

University of Liège

Frank Delvine

Gembloux Agro-Bio Tech

Frédéric Nguyen

University of Liège

Article

Keywords:

Posted Date: March 3rd, 2026

DOI: https://doi.org/10.21203/rs.3.rs-8899213/v1

License: This work is licensed under a Creative Commons Attribution 4.0 International License.
Read Full License

Additional Declarations: No competing interests reported.

Disentangling the Sources of Spectral Induced Polarization of Microbial Systems: Experiments in Non-Geological Media

Satoshi Izumoto[1,*], Frank Delvine[2], and Frédéric Nguyen[1]

[1]Faculty of Applied Sciences, Urban and Environmental Engineering Department, University of Liège, Liège, Belgium
[2]Terra Research and Teaching Centre, Microbial Processes and Interactions (MiPI), Gembloux Agro-Bio Tech, University of Liège, Gembloux, Belgium
[*]satoshi.izumoto@hotmail.co.jp

ABSTRACT

This study investigates the origin of spectral induced polarization (SIP) signals associated with microbial systems, aiming to distinguish direct microbial electrical effects from indirect geochemical processes. Although SIP has been proposed for detecting subsurface microbial activity, its interpretation is complicated by overlapping polarization mechanisms. We therefore performed controlled experiments in simplified, non-geological environments to isolate the roles of microbial presence, attachment, and activity. Using a custom millifluidic chip, SIP measurements were conducted with *Pseudomonas putida* KT2440 under three configurations: bacteria suspended in solution, bacteria attached to metal surfaces, and bacteria affecting SIP through redox reactions. Bacterial cells in suspension did not produce a measurable SIP response: phase shifts were indistinguishable from those of the background medium, despite small increases in bulk conductivity. Reanalysis of previous studies indicates that interpretations based solely on imaginary conductivity can be misleading, and that phase shift is the more reliable indicator. Likewise, bacterial attachment to metal surfaces did not modify the SIP response, even though microscopy confirmed surface colonization. In contrast, strong and time-dependent SIP signals were observed when iron was immersed in oxygenated media, closely tracking oxygen consumption and attributable to surface oxidation. When oxygen was removed—by microbial respiration or chemical scavenging—the change in SIP response was significantly reduced, and systems with and without bacteria behaved similarly. Numerical simulations with redox-modified boundary conditions reproduced these trends and linked SIP evolution to changes in surface capacitance and electron transfer. Overall, SIP is sensitive not to microbial cells themselves, but to microbially mediated redox processes involving conductive materials.

Introduction

Microorganisms play a major role in elemental cycling on Earth. Recent advances have demonstrated the feasibility of remotely detecting bacterial gene expression at soil surfaces using a range of reporter-based strategies, including hyperspectral reporters[1]. However, mapping microbial activity within the subsurface—where direct optical access is precluded—remains a major unresolved challenge. Among geophysical techniques, Spectral Induced Polarization (SIP) and time-domain Induced Polarization (IP) have emerged as promising methods for detecting microbial activity under various conditions[2,3]. These techniques characterize the dielectric properties of the subsurface: SIP applies a sinusoidal voltage and analyzes the frequency-dependent response, while IP measures the voltage decay after switching off a direct current pulse. Despite their potential, numerous challenges remain before SIP and IP can be reliably applied in practical field settings.

Early laboratory investigations were driven by the hypothesis that microbial activity would alter the IP response of surrounding materials[4]. This perspective gradually evolved into a more targeted question: can SIP/IP measurements be used to directly detect microbial activity? To explore this, many studies have examined SIP/IP responses during processes such as biomineralization[5–9], biofilm formation[10–12], bioclogging[13,14] and biogeochemical transformations like contaminant degradation[15–19] and other microbial processes such as redox reaction, adsorption and microbial induced chemical reactions[13,20–23]. These experimental results are encouraging, particularly because no other geophysical technique currently offers a reliable means of detecting microbial activity. Some field studies even report that SIP/IP measurements successfully identified zones of microbial activity in contexts involving decontamination[24–28] or mineral precipitation[29,30]. However, many of these successes have occurred in settings where prior subsurface information—such as the expected reactions—was already available[27,29,30]. In such cases, anomalies in SIP/IP data are interpreted through correlations with known or expected zones of microbial activity rather than through causal mechanisms. The method is far less frequently used in environments without prior knowledge, limiting

its broader application as an exploratory tool. To advance the technique's applicability, several key challenges must be addressed.

First, interpreting SIP/IP measurements requires careful consideration. A variety of processes can contribute to the observed polarization response, including the presence of conductive metals and clays[2,3], pore clogging by non-conductive minerals[31], and polarization associated with nanoporous structures[32]. As a result, it is often challenging to disentangle the specific source of the SIP/IP signal.
Second, some studies have reported changes in the imaginary part of the complex conductivity (σ'') as an indicator of microbial activity. However, because σ'' is related to the real part of conductivity (σ') and the phase shift (ϕ) through the relation $\sigma'' = \sigma' \tan\phi$, an increase in σ'' can arise solely from an increase in solute conductivity—even if ϕ remains unchanged. In such cases, it is not possible to distinguish changes due to microbial activity from those caused by abiotic processes. Therefore, without a corresponding analysis of the phase shift, interpretations based solely on σ'' may be misleading.

Third, the underlying physics of SIP/IP signals associated with microbial activity remain an area of active investigation. While some theoretical models propose mechanisms such as electrical double layer polarization[33], experimental validation under controlled conditions is still limited. A contributing factor is that many laboratory studies are conducted in complex porous or geological media, where interactions between microbes and mineral surfaces —as well as potential pore clogging due to biofilm formation— introduce additional variables that complicate both measurement and interpretation. To date, experiments performed in bulk solutions[34,35] —where such complexities are reduced— have not clearly demonstrated SIP responses directly attributable to microbial presence. This issue is revisited in detail in the Results and Discussion section.
Finally, we note a likely publication bias: studies reporting the absence of SIP/IP response are rarely published, which may skew the current understanding toward overestimating the detectability of microbial processes by SIP/IP.
In light of these limitations, this study aims to disentangle the fundamental sources of SIP responses associated with microbial activity. We conduct controlled experiments in a simplified setup to determine the conditions under which microbial activity produces a detectable SIP response and, just as importantly, when it does not. Our interpretations are further supported by numerical simulations designed to clarify the mechanisms involved.

1 Methods

1.1 Design of the chip

To measure microbial activity in a simplified configuration —free from geological materials such as sand and rocks, but optionally including metal inclusions within the channel— we developed a compact device referred to as a millifluidic chip. This chip is designed for easy assembly using standard laboratory equipment. The chip consists of three transparent polymethyl methacrylate (PMMA) plates: a top plate, a middle plate, and a bottom plate (Fig.1a). The bottom plate is a flat solid sheet. The middle plate is patterned with a cutout that serves as the fluid channel. The top plate contains several features: electrode ports and two fluid inlet/outlet holes for tubing connections. Electrodes are secured onto the top plate using epoxy resin. To minimize measurement interference, the potential electrodes are retracted from the main flow path using a perpendicular borehole (2 mm in diameter, 4 mm in length), following the design criteria of Zimmermann et al. (2008)[36]. To assemble the chip, we used parafilm as a thermally activated adhesive. Strips of parafilm were placed between the top/middle and middle/bottom plates. The entire structure was then clamped and heated at 60°C for approximately 30 minutes, during which the parafilm softened and adhered the layers together. For disassembly, the chip was gently reheated to make the parafilm sticky and allow the layers to separate.

1.2 Reporter strain

The bacterial strain used in this study is a derivative of *Pseudomonas putida* KT2440 cured of the TOL plasmid (kindly provided by the de Lorenzo laboratory, Spain). To facilitate cell detection, the strain was transformed with a constitutively expressed fluorescent reporter. The reporter gene (Yellow Fluorescent Protein - YFP) was carried on the replicative plasmid pSEVA227Y (KmR; RK2 origin of replication; pBG17–YFP) and introduced into the cells by electroporation[37]. Working seed stocks were prepared by storing the strain in 25% (v/v) glycerol at -80 °C in 2 mL cryovials. Prior to experiments, a single colony was used to inoculate 10 mL of lysogeny broth (LB) medium (10 g /L NaCl, 5 g/L yeast extract, and 12 g/L tryptone). The growth conditions for each experiment are described in the corresponding subsections below.

1.3 Measurement of Microbes in Suspension

To investigate whether suspended bacteria (*P. putida* KT2440) alone can generate a measurable SIP response, we injected bacterial suspensions into the millifluidic chip. *P. putida* KT2440 with yellow fluorescent protein (YFP) was cultured in three

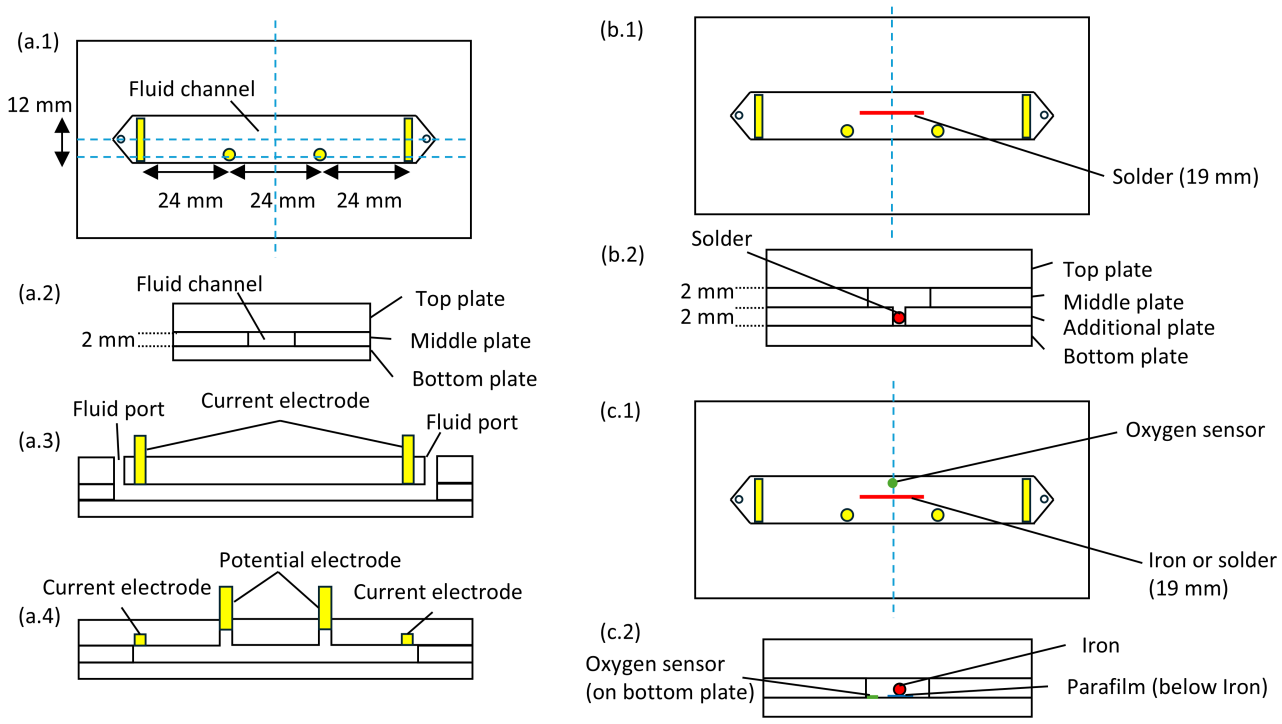


Figure 1. Design of the millifluidic chip. (a.1) Top view of the chip layout. Electrodes are shown in yellow. Dotted blue lines indicate the locations of cross-sections displayed in (a.2), (a.3), and (a.4). (a.2) Cross-section along the vertical dotted line in (a.1). (a.3) Cross-section along the horizontal dotted line at the center of the fluid channel in (a.1). (a.4) Cross-section along the horizontal dotted line at the bottom of the fluid channel in (a.1). (b.1) Top view of the experimental setup for bacterial attachment. The dotted blue line indicates the cross-section shown in (b.2). (b.2) Cross-section along the vertical dotted line in (b.1). (c.1) Top view of the experimental setup for oxygen consumption measurements. The dotted blue line indicates the cross-section shown in (c.2). (c.2) Cross-section along the vertical dotted line in (c.1).

separate flasks at 30 °C for 7 hours on a shaker (150 rpm). The optical densities (OD) at 600 nm, measured after 10-fold dilution, were 0.338, 0.335, and 0.273. Each of the original suspensions was injected into the chip, and the SIP response was measured individually for each sample.

1.4 Attachment of Microbes on Metal Surfaces

To assess how microbial attachment to metal surfaces affects the SIP response, we conducted a controlled experiment using metal solder wires (Sn60/Pb40). LB agar was prepared in six wells. *P. putida* KT2440 with YFP (OD = 1.314 after 3 hours of incubation) was inoculated onto the surface of three wells, while the remaining three were left uninoculated as controls. A piece of solder wire (diameter: 0.71 mm; length: 19 mm), pre-sterilized, was placed in each well. All wells were incubated at 30 °C for 23 hours to allow microbial growth and attachment. After incubation, each solder sample was transferred into the chip filled with LB medium. SIP measurements were conducted for all six wires—three with expected bacterial attachment and three without. Microscopic imaging was used to confirm bacterial attachment. To assess the SIP signal in the absence of surface-attached microbes, the same wires were then immersed in boiling water for 1 minute and 30 seconds to remove the bacteria. Microscopic inspection confirmed the absence of remaining cells on the surface, after which SIP measurements were repeated on the cleaned solder samples. To accommodate rapid SIP measurements during this experiment, we used a modified version of the millifluidic chip designed for easier assembly (Fig.1b). In this version, an additional PMMA plate with a small rectangular slot for holding the solder was inserted between the middle and bottom plates. Instead of parafilm, silicone grease was applied along the interfaces to prevent leakage, and the chip was clamped securely.

1.5 Oxygen Consumption and Indirect SIP Response from Microbial Activity

We evaluated whether microbial activity can indirectly influence SIP signals via redox processes. In the primary experiment (Iron–Bacteria), a soft black iron wire was placed in a millifluidic chip filled with LB medium inoculated with *P. putida* KT2440 with YFP (Fig.1c). Prior to loading into the chip, bacterial cultures were grown in LB medium for 4–8 h at 30 °C under shaking conditions (150 rpm), then diluted with LB medium to an optical density at 600 nm of approximately 0.25 (OD_{600} = 0.279, 0.265, and 0.236 for triplicate experiments). The wire was fixed to the bottom PMMA plate using heated parafilm. Oxygen concentration was monitored using an optical oxygen sensor (Oxygen Sensor Spots PSt3/PSt6, Fig.1c.1), and SIP measurements were performed every 15 minutes for 200 minutes. Microbial respiration was expected to deplete oxygen, thereby suppressing iron oxidation and influencing the SIP response. To isolate the role of oxygen and microbial activity, we performed comparative measurements under the following conditions: (1) Iron - O_2: Iron in sterile LB medium without bacteria (no microbial oxygen consumption). (2) Iron - No O_2 (LB): Iron in LB medium chemically deoxygenated using sodium sulfite (0.0008 g/mL) and cobalt sulfate (0.0003 g/mL). (3) Iron - No O_2 (NaCl): Iron in chemically deoxygenated NaCl solution (8.33 mg/mL), adjusted to match the electrical conductivity of LB medium. (4) Iron - No O_2 (Epoxy): Same as (2), but with the freshly cut ends of the iron wire sealed using epoxy to prevent edge oxidation. (5) Solder - O_2: Solder wire in sterile LB medium (used as a less reactive control metal). As a reference for background oxygen dynamics unrelated to microbial or electrochemical activity, we also monitored oxygen levels in sterile LB medium without metal or bacteria.

1.6 Simulation

Recent theoretical and experimental studies have investigated the polarization behavior of metal grains, providing a robust theoretical foundation supported by experimental evidence[38]. Building upon this framework, Izumoto (2023)[39] developed a numerical modeling approach, which was further extended in Izumoto and Nguyen (2025)[40] for plant root systems. We adopt and extend them by incorporating redox reactions at the metal–fluid interface. We begin by briefly reviewing the theoretical basis. Outside the metal grain, the electric current in the bulk fluid is governed by Ohm's law:

$$\boldsymbol{j} = -\sigma_0 \nabla \phi \tag{1}$$

where $\boldsymbol{j}$ ($\mathrm{A\,m^{-2}}$) is the current density vector, σ_0 ($\mathrm{S\,m^{-1}}$) is the bulk electrical conductivity, and ϕ (V) is the electric potential. The conservation of charge (i.e., zero divergence of current) leads to:

$$\nabla \cdot (\sigma_0 \nabla \phi) = 0 \tag{2}$$

On the surface of the metal grain, charge accumulation is described by:

$$\frac{d\rho}{dt} = \boldsymbol{j} \cdot \boldsymbol{n} \tag{3}$$

where ρ ($\mathrm{C\,m^{-2}}$) is the excess surface charge density, and $\boldsymbol{n}$ is the outward unit normal vector. This relation reflects the conservation principle that current flowing perpendicular to the surface modifies the local charge density. The surface charge is related to the potential via the surface capacitance:

$$\rho = C_0(\phi - \bar{\phi}) \tag{4}$$

where C_0 ($\mathrm{F\,m^{-2}}$) is the surface capacitance, and $\bar{\phi}$ is the average potential over the grain surface. In our experimental configuration, where the metal grain is centered in the channel, we assume $\bar{\phi} = 0$, simplifying Eq.4 to a direct proportionality between local potential and surface charge. This relation is consistent with basic principles of electrostatics and charge storage. Combining Eqs. 1, 3, and 4, we arrive at the governing equation for potential evolution at the metal surface:

$$C_0 \frac{\partial \phi}{\partial t} = -\sigma_0 \frac{\partial \phi}{\partial r} \tag{5}$$

where $\partial/\partial r$ denotes the spatial derivative normal to the surface. The model features a single fitting parameter, C_0, representing the surface's charge storage capacity. Izumoto (2023)[39] extended this framework to include redox reactions at the grain–fluid interface. Redox processes enable electron exchange between the metal and surrounding fluid, introducing an additional current contribution. Incorporating this effect into Eq.5, we obtain:

$$C_0 \frac{\partial \phi}{\partial t} - \sigma_s \frac{\partial \phi}{\partial r} = -\sigma_0 \frac{\partial \phi}{\partial r} \tag{6}$$

where σ_s ($\mathrm{S\,m^{-1}}$) quantifies the contribution of redox-driven current. Comparing Eq.5 and Eq.6, we see that redox reactions effectively reduce the surface polarization by replacing σ_0 with $\sigma_0 - \sigma_s$. This change results in a shift in the frequency of maximum polarization response[39]:

$$f_{pr} = \frac{\sigma_0 - \sigma_s}{\sigma_0} f_p \tag{7}$$

where f_{pr} ($\mathrm{s^{-1}}$) is the peak frequency with redox coupling, and f_p is the peak frequency without it. This decrease in peak frequency under redox conditions has been observed experimentally with minimal change in polarization magnitude[41]. That study involved Fe^{2+}/Fe^{3+} redox chemistry, where the redox current was well-approximated by the potential gradient near the surface, implying negligible activation energy. In contrast, our experiments involve iron immersed in LB medium, where oxygen is the primary oxidant. In this case, the redox reaction is likely activation-limited, and the driving force is better approximated by the local surface potential itself, rather than its gradient. Accordingly, we modify the governing equation to:

$$C_0 \frac{\partial \phi}{\partial t} = -\alpha\phi - \sigma_0 \frac{\partial \phi}{\partial r} \tag{8}$$

where α ($\mathrm{S\,m^{-2}}$) represents an electron transfer on the surface due to redox reaction, acting as a sink term that diminishes surface charge accumulation. We assume a sinusoidal applied potential and derive equations for frequency domain. In the bulk fluid, Eq.2 separates into:

$$\nabla \cdot (\sigma_0 \nabla \phi') = 0 \tag{9}$$

$$\nabla \cdot (\sigma_0 \nabla \phi'') = 0 \tag{10}$$

where ϕ' and ϕ'' denote the real and imaginary parts of the potential, respectively. From Eq.8, on the metal surface, the corresponding boundary conditions are:

$$\phi' = -\frac{\sigma_0}{2\pi f C_0} \left(\frac{\partial \phi''}{\partial r} - \frac{\alpha}{\sigma_0} \phi'' \right) \tag{11}$$

$$\phi'' = \frac{\sigma_0}{2\pi f C_0} \left(\frac{\partial \phi'}{\partial r} - \frac{\alpha}{\sigma_0} \phi' \right) \tag{12}$$

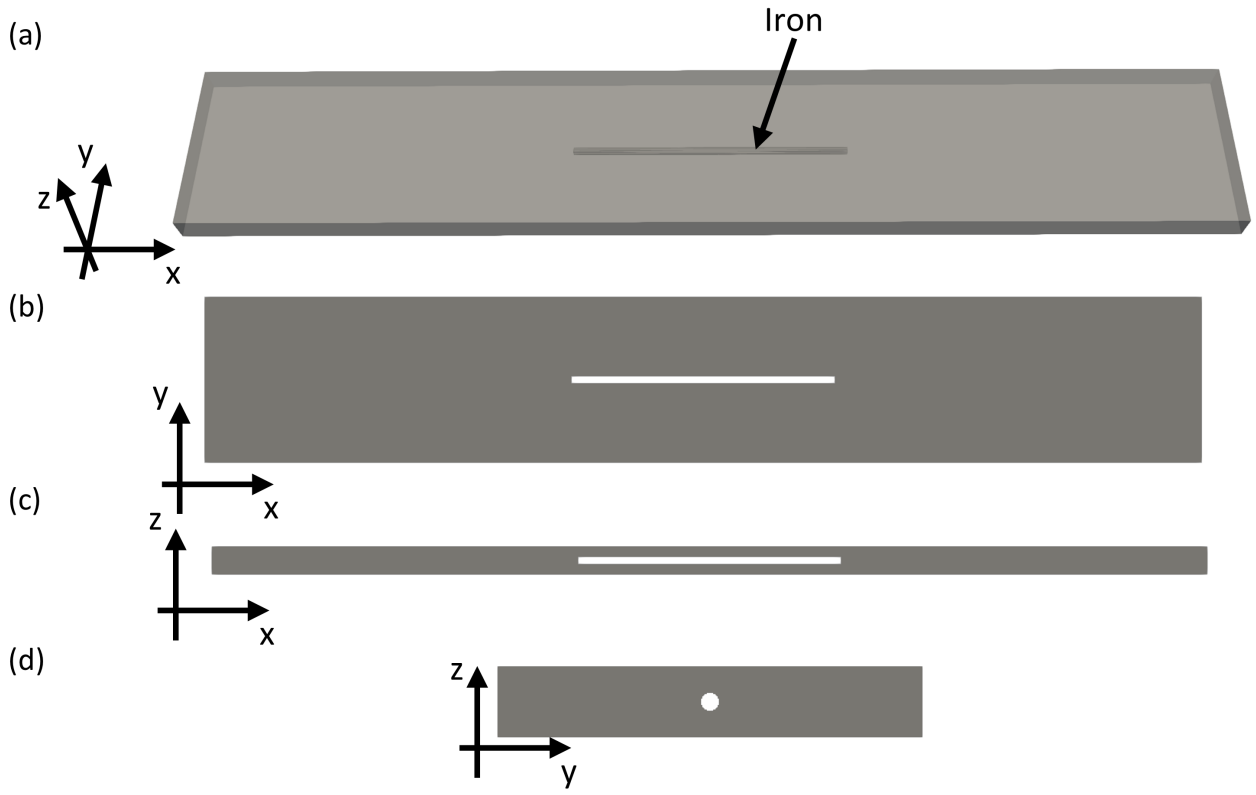


Figure 2. Schematics of the simulation setup. (a) Three-dimensional view of the simulation domain, showing the iron inclusion centered within the fluid channel. (b) Cross-section in the x–y plane, with the iron region indicated in white. (c) Cross-section in the x–z plane, illustrating the vertical placement of the iron inclusion. (d) Cross-section in the y–z plane, showing the channel height and iron geometry.

To solve these equations numerically, we updated the surface potential iteratively. At iteration step $n+1$, the surface potentials were updated as:

$$\phi'_{n+1} = \phi'_n + \delta_i \left(\phi'_n - \left(-\frac{\sigma_0}{2\pi f C_0} \left(\frac{\partial \phi''_n}{\partial r} - \frac{\alpha}{\sigma_0} \phi''_n \right) \right) \right) \tag{13}$$

$$\phi''_{n+1} = \phi''_n + \delta_i \left(\phi''_n - \frac{\sigma_0}{2\pi f C_0} \left(\frac{\partial \phi'_n}{\partial r} - \frac{\alpha}{\sigma_0} \phi'_n \right) \right) \tag{14}$$

Here, δ_i is a relaxation parameter chosen empirically to ensure numerical stability, typically between 10^{-4} and 10^{-3} depending on frequency. The model was implemented in OpenFOAM (https://openfoam.org/).

The simulation domain replicates the experimental geometry, consisting of a cylindrical metal object (0.5 mm diameter, 19 mm length) placed centrally in a fluid channel (Fig.2, 720 mm $\times$ 120 mm $\times$ 2 mm in x, y, and z directions, respectively). Boundary conditions were as follows: $\phi' = \pm 1$ on the current injection faces, zero-gradient for ϕ' on all other boundaries except the metal surface, and zero-gradient for ϕ'' everywhere except the metal surface. The principal advantage of this modeling approach[38–40] is its simplicity. By representing the metal–fluid interface as a surface capacitance, the model avoids resolving ion distributions within the electrical double layer (typically on the nanometer scale), as required in more complex models based on the Poisson–Nernst–Planck (PNP) framework[42,43]. As such, this method is well-suited for cases where macroscopic geometry plays an essential role. For studies focused on nanoscale electrochemical phenomena, however, PNP modeling would be necessary.

2 Results and discussion

2.1 Analysis of microbial cells in suspension in the liquid phase

The phase shifts observed in the three measurements of *P. putida* suspensions in LB medium overlap with those of the background (LB medium without bacteria), indicating that the presence of bacterial cells—even at high density—does not induce a measurable SIP response (Fig.3a). A modest increase of approximately 10% in the absolute conductivity was noted (Fig.3b), which can be attributed to changes in the bulk fluid properties due to bacterial growth, rather than to polarization phenomena.

Previous studies examining SIP responses of bacterial suspensions in the relevant frequency range remain limited. Although many investigations have explored the effects of microbial activity on SIP signals, their results are often influenced by surrounding complex media, such as geological materials, making it difficult to isolate the microbial contribution. For this reason, we restrict our discussion to studies conducted in the absence of porous or mineral matrices to focus on the intrinsic origins of the SIP response.

Additionally, many studies in colloid and microbiology have employed two-electrode configurations, which are prone to electrode polarization effects—especially at frequencies below tens of kilohertz. We therefore exclude such studies from this discussion. Among the limited relevant literature, one thesis study[35] reported the absence of SIP peaks in bacterial suspensions, which is consistent with our findings (Fig.4). In contrast, Zhang et al. (2014)[34] reported the presence of a SIP response in bacterial suspensions at much lower cell concentrations than those used in our experiments, based on the imaginary part of conductivity. In the following discussion, we argue that the phase shift is a more reliable indicator of polarization and examine this apparent discrepancy by focusing on phase shift rather than on the imaginary component of conductivity.

In their interpretation, Zhang et al. (2014)[34] based the identification of microbial SIP signals on changes in the imaginary part of the complex conductivity (σ''). However, since their experiments also showed changes in the real component (σ'), the interpretation of σ'' alone is insufficient. This is because σ'' may increase as a result of increased σ' even when the phase angle ϕ remains unchanged according to the relation $\sigma'' = \sigma' \tan\phi$. Given that ϕ is rarely exactly zero in practice—due to instrumentation limits or minor background polarization—any increase in σ' (e.g., due to fluid conductivity changes) can lead to an increase in σ'' without invoking additional polarization mechanisms.

Moreover, measurement uncertainty in SIP experiments is conventionally defined in terms of the phase angle ϕ, which directly reflects the time delay (or advance) of the sinusoidal voltage response. Therefore, ϕ should be the central parameter for interpreting SIP measurements. To re-evaluate the conclusions of Zhang et al. (2014)[34], we re-analyzed their published data to extract ϕ directly from their reported complex conductivity values.

The re-analysis revealed that ϕ values for the bacterial suspensions were within a few milliradians (Fig.5)—close to the detection limit of modern SIP systems under ideal conditions[36]. Furthermore, the phase values for the bacterial suspensions fell between those of two background measurements that did not contain any polarizing material. Notably, ϕ showed minimal dependence on bacterial concentration and even slightly increased (i.e., less polarization) as the concentration increases at frequencies above 1 Hz. Below 1 Hz, the trend was unclear. These findings suggest that the SIP signal observed by Zhang et al. (2014)[34] does not originate from the bacterial cells and is consistent with our conclusion that bacterial suspensions alone do not produce a significant SIP response.

Although not directly comparable to our setup, we also examined the data from Zhang et al. (2014)[34] involving bacteria in sand (Fig.5). In our view, the reported phase peaks are rather broad plateaus and fell within a few milliradians—again, close to the measurement resolution. Furthermore, the phase increased (i.e., less polarization) with increasing bacterial concentration above 1 Hz, and the trend at lower frequencies was ambiguous. Across five orders of magnitude in frequency, the phase never approached zero, which raises the possibility of a non-negligible background signal affecting the measurement. These observations further support our interpretation that the bacterial cells themselves do not induce a discernible SIP response.

It is also important to emphasize the susceptibility of SIP measurements to experimental artifacts. Poorly controlled experimental setups—such as those with high electrode contact resistance—can introduce substantial noise and frequency-dependent distortions, particularly in the imaginary component of the signal. However, such artifacts are more likely to produce spurious SIP responses than to suppress real ones. Therefore, we argue that while claims of SIP presence must be interpreted with caution, the absence of a phase shift (i.e., no difference from background) constitutes a more robust and reliable conclusion.

2.2 Microbes Attached to Metal Surfaces

Microscopic imaging confirmed the presence of bacterial attachment to the metal surface prior to treatment (Fig.6a,c), and the successful removal of bacteria following boiling (Fig.6b). Control experiments—conducted using solder samples that were not exposed to bacteria—showed negligible changes in both phase shift and electrical conductance before and after boiling (Fig.7), confirming that the boiling process itself does not alter the SIP response of the metal. In experiments where bacteria were allowed to attach to the solder surface, the measured SIP response (in both phase shift and conductivity) was nearly identical to

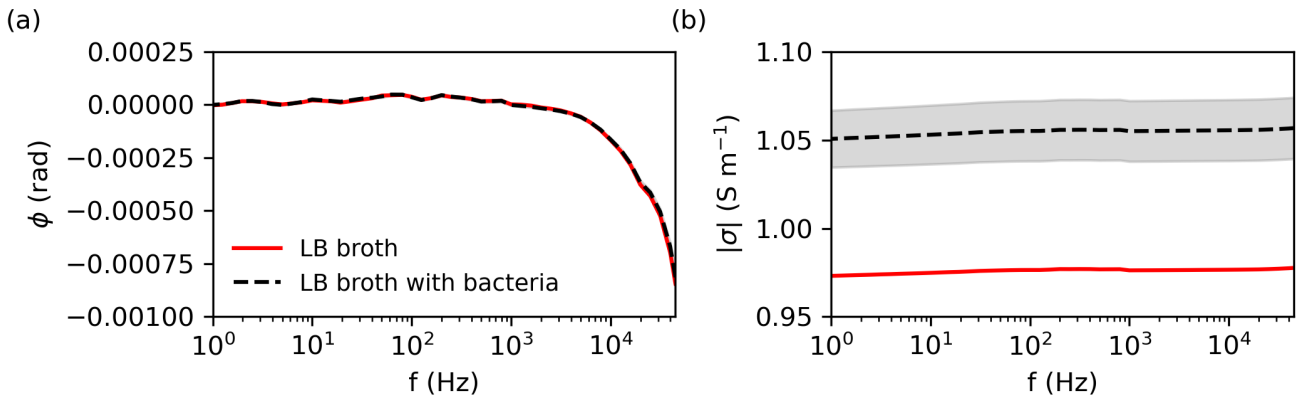


Figure 3. Experimental results of the SIP response in LB medium and LB medium containing suspended bacteria (*P. putida* KT2440). (a) Phase shift (ϕ) as a function of frequency. (b) Absolute conductivity ($|\sigma|$). In both panels, the shaded gray region indicates one standard deviation around the mean of replicate measurements.

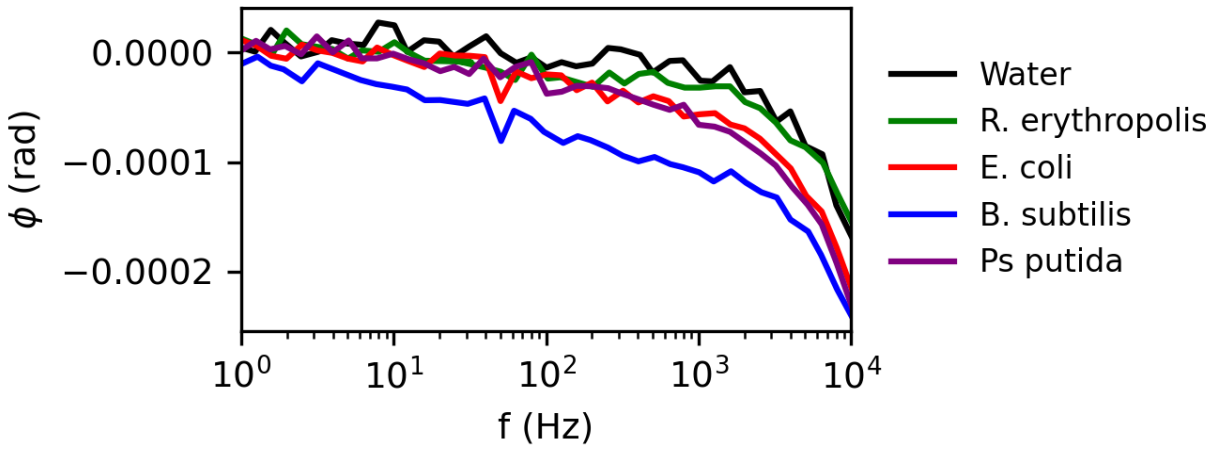


Figure 4. Phase shift (ϕ) of bacterial suspension of different bacteria species, calculated from the experimental data reported in Pilawski (2019). The values were derived from the original complex conductivity data to directly assess the presence or absence of polarization response.

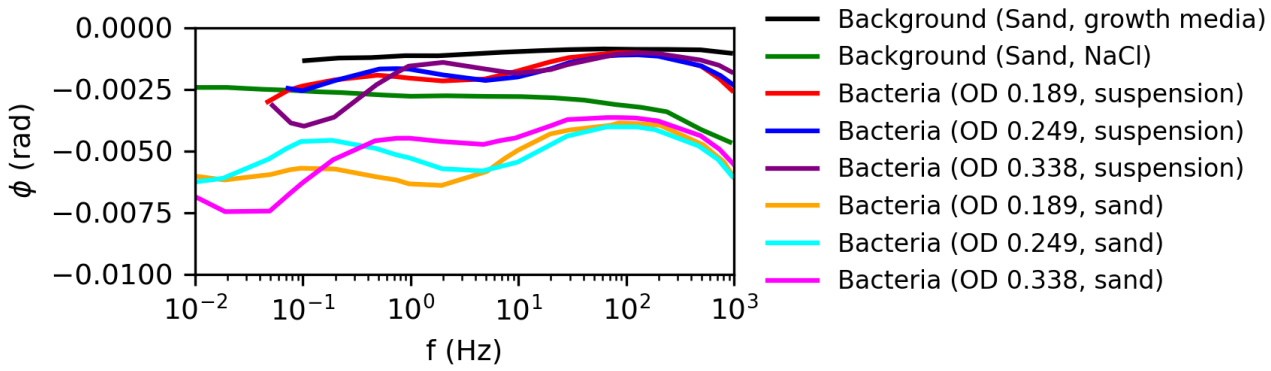


Figure 5. Phase shift (ϕ) calculated from the experimental data of Zhang et al. (2014). The values were derived from the reported complex conductivity measurements to evaluate the presence of a polarization response in bacterial suspensions and bacterial–sand mixtures. OD represents optical density measured at 600 nm.

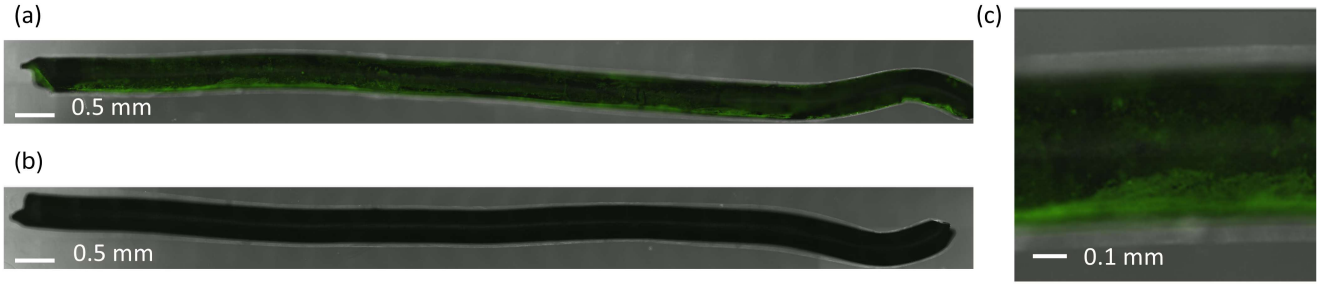


Figure 6. Microscopic images from the bacterial attachment experiment. (a) Bacteria attached to the surface of the solder were detected based on the YFP fluorescent reporter (here visualized on the green channel). (b) The same solder sample after boiling, showing the removal of surface-attached bacteria. (c) Close-up view of the solder surface in (a).

that of the control condition (Fig.7). This result indicates that bacterial attachment to the metal surface does not influence the SIP response.

These results can be interpreted from a conceptual standpoint. If a conductive metal surface is coated with a resistive material, the resulting SIP response would be expected to change. In our case, earlier experiments showed that bacteria in suspension do not generate a measurable SIP signal (Fig.3), indicating that bacterial cells behave as non-polarizable, resistive inclusions—consistent with the insulating nature of their lipid bilayers. Based on this, one might expect that the attachment of bacteria to the metal surface would alter the SIP response. However, no such change was observed. This apparent discrepancy can be explained by the shape and attachment mode of the bacteria: because bacterial cells are ellipsoidal, they likely adhere to the surface at discrete points rather than forming a continuous insulating layer. As a result, much of the metal interface remains exposed, allowing the original polarization behavior to persist.

These findings suggest that previously reported SIP signals associated with microbial activity are unlikely to originate from physical interactions between bacterial cells and metallic surfaces. Instead, other mechanisms—such as microbially mediated geochemical processes—are more plausible explanations.

2.3 Microbial Activity Coupled with Oxidation of Metal

We first measured the background oxygen concentration in sterile LB medium without iron (Background), which showed a slight decrease over time—likely due to minor consumption by the oxygen sensor itself (Fig.8a). When we introduce iron in the chip (Iron - O_2 condition), oxygen concentration dropped rapidly at first and then decreased more slowly (Fig.8a), showing that iron is oxidized over time.

During this period, the phase shift (ϕ) exhibited a clear peak in the 10–100 Hz range, and this response evolved over time (example in Fig.9a). Specifically, the peak phase (ϕ_p) and peak frequency (f_p) decreased rapidly at first, then more gradually-

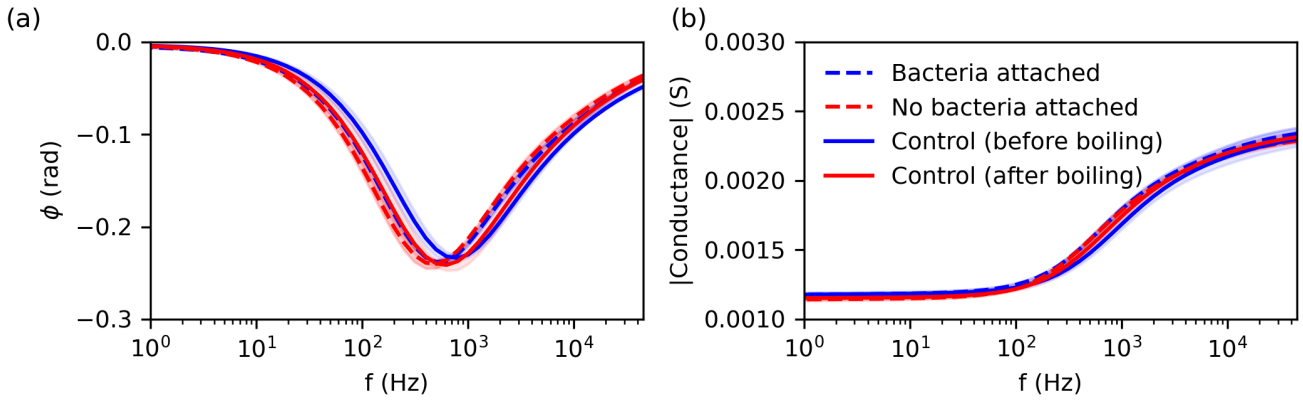


Figure 7. SIP response of bacterial attachment on solder. (a) Phase shift (ϕ) and (b) absolute conductance measured before and after bacterial attachment.

mirroring the temporal evolution of the oxygen concentration (Fig.8b,c,d,e). The absolute conductivity ($|\sigma|$) remained close to 1 S m^{-1} at low frequencies (Fig.9b), consistent with the expected conductivity of LB medium. These trend of oxygen concentration and SIP response suggests that iron oxidation is the dominant driver of the observed changes in SIP response.

In contrast, when bacterial suspension was introduced (Iron - Bacteria condition), the oxygen had already been consumed within minutes prior to injection into the chip, resulting in near-zero oxygen concentration at the start of the measurement (Fig.8a). As a result, iron oxidation was suppressed, and the SIP response changed less over time (Fig.8c,e), confirming that the presence of oxygen and microbial activity is critical for SIP signal evolution. The smaller ϕ_p (i.e., stronger polarization) observed in the Iron - Bacteria condition (Fig.8b) will be discussed in relation to the simulation results in a later section.

To further isolate the effect of microbial activity from oxygen concentration, we performed an additional experiment in which oxygen was depleted using a chemical scavenger (Na_2SO_3 and $CoSO_4$) prior to injecting LB medium into a chip containing an iron wire (Iron - No O_2 condition). Oxygen measurements confirmed near-zero concentrations from the start (Fig.8a). Importantly, the only difference between the Iron + Bacteria condition and the Iron - No O_2 condition was the presence of microbes. The ϕ_p, f_p and $f_p/f_{p,0}$ were overlapping for these two conditions (Fig.8b,d,e). The difference in $\Delta\phi$ at the end of the experiment between these two conditions was approximately 15 mrad on average—comparable to one standard deviation across triplicates, and thus likely not statistically significant (Fig.8c). Thus, we did not see any significant difference solely due to the presence of bacterial. However, both of these conditions differed significantly from Iron + O_2 condition (Fig.8b,c,d,e), in which ϕ_p was larger, f_p was smaller, and $\Delta\phi$ changed more markedly. These results suggest that microbial activity influences the SIP response, in the presence of metal, only indirectly—primarily through oxygen consumption that suppresses iron oxidation. This conclusion is consistent with our earlier findings showing that bacteria in bulk suspension and on metal surfaces do not themselves induce SIP responses.

Notably, even under oxygen-depleted conditions, the SIP response of iron still changed over time. This raises the question of whether factors other than oxygen-driven iron oxidation could be responsible. We first hypothesized that some reaction at the freshly cut ends of the iron wire might contribute significantly. To test this, we sealed both ends of the wire with epoxy resin and repeated the measurement under oxygen-depleted LB medium conditions (Iron - No O_2 (Epoxy)). However, the SIP response still showed significant decreases in $\Delta\phi_p$ and $f_p/f_{p,0}$ (Fig.10), suggesting that there is a significant contribution other than wire ends.

Next, we hypothesized that components of LB medium might act as alternative oxidants. To examine this, we repeated the oxygen-depleted experiment using a NaCl solution with matched conductivity (Iron - No O_2 (NaCl)). The SIP response again showed substantial changes in $\Delta\phi_p$ and $f_p/f_{p,0}$ (Fig.10), indicating that constituents of LB medium were also not responsible for the observed signal.

Based on these results, we argue that even trace amounts of oxygen are sufficient to induce surface oxidation of iron, resulting in detectable changes in SIP response. Conceptually, this is reasonable: oxidation limited to the grain surface requires only minimal oxygen, as bulk metal transformation is not necessary to alter interfacial polarization. This explanation is further supported by our measurements on solder wire, which is significantly less susceptible to oxidation.

In the solder experiments, oxygen consumption was negligible and closely followed the background trend (Fig.8a). Correspondingly, changes in maximum ϕ_p and $f_p/f_{p,0}$ were much smaller than those observed in the iron cases (Fig.8b,c,d,e). Nevertheless, slight changes were still detectable, likely due to limited surface oxidation—highlighting the sensitivity of SIP measurements to

subtle surface alterations. These findings reinforce the hypothesis that even very low levels of residual oxygen can produce measurable changes in SIP response through surface oxidation processes.

2.4 Simulation of SIP Response from Iron Oxidation

We simulated the SIP response associated with iron oxidation to match experimental results by adjusting two parameters: the surface capacitance (C_0, in $\mathrm{F\,m^{-2}}$) and the electron transfer on the surface due to redox reaction (α, in $\mathrm{S\,m^{-2}}$). Examples of the simulated potential fields and electric current at the peak frequency are presented in Fig.11. The real part of the potential exhibited extrema at the current injection and outlet boundaries (Fig.11a), while the imaginary part showed localized maxima and minima near the edges of the iron inclusion (Fig.11b). These spatial patterns are consistent with prior modeling studies[39]. The real component of the electrical current density also indicated partial current penetration into the iron, with the highest current density concentrated along the edges (Fig.11c).

To compare simulations with experimental data, we sampled the potential at the same electrode positions used in the measurements. The simulation successfully reproduced both the peak phase shift and the peak frequency, although the spectral shape was somewhat narrower than that observed experimentally (Fig.12a). The absolute conductivity ($|\sigma|$) also followed trends similar to those recorded in the experiments (Fig.12b).

The fitted values of C_0 showed an increasing trend over time, consistent with the progressive alteration of surface properties during the oxidation process (Fig.12). The redox-driven electron transfer, α, decreased from approximately 300 to 100 $\mathrm{S\,m^{-2}}$ during the course of the experiment (Fig.12). This trend aligns with the expected physical mechanism: higher electron transfer rates are anticipated at earlier stages of oxidation, when surface reactions are more intense.

To further quantify the temporal evolution of α based on experimental observations, we first ran simulations with fixed α values of 50, 100, 150, 200, 250, and 300 $\mathrm{S\,m^{-2}}$. Because simulating a full spectrum for each α is computationally expensive, we fitted a quadratic curve around the spectral peak to interpolate the peak phase shift (ϕ_p) from sparse frequency data. This enabled us to construct a relationship between α and ϕ_p, which we then used to estimate effective α values directly from the experimental measurements (Fig.13a). Note that C_0 only influences the frequency dependence of the response, while the magnitude of ϕ depends on α (Eq.11,12). Therefore, α can be estimated from the observed ϕ_p without needing to account for variations in C_0.

The estimated α values support our experimental interpretation. The oxidation rate (reflected by α) was consistently highest in the Iron - O_2 condition, while it was significantly lower—but still measurable—in both the Iron - Bacteria condition and Iron - No O_2 condition (Fig 13b). Over time, α decreased in all cases: for the Iron - O_2 condition, it declined to roughly one-third of its initial value, while in the other two conditions it dropped to about half (Fig 13b). These results confirm that the presence of oxygen accelerates oxidation, and that oxidation rates diminish as the experiment progresses.

Finally, it is noteworthy that a positive, nonzero α was still necessary to reproduce the experimental data at later times. This supports the interpretation that even small residual amounts of oxygen can sustain a measurable degree of oxidation—and thus a persistent SIP response—throughout the experimental period.

3 Conclusion

This study aimed to clarify the conditions under which microbial activity contributes to spectral induced polarization (SIP) signals by disentangling the roles of microbial presence, attachment, and activity from those of geochemical processes—specifically, metal oxidation.

We first demonstrated that *P. putida* KT2440, whether suspended in bulk solution or attached to metal surfaces, does not generate a measurable SIP response. These findings were supported by both our own experiments and a critical reanalysis of prior studies. The observed lack of phase shift in these cases reinforces the interpretation that the microbial body itself—composed largely of insulating lipid membranes—acts as a non-polarizable inclusion in the frequency range of SIP measurement.

In contrast, we observed strong and time-evolving SIP signals when iron was immersed in oxygenated LB medium. These changes, including maximum phase shift and peak frequency, closely tracked the dynamics of oxygen consumption and are attributed to interfacial polarization caused by iron surface oxidation. When oxygen was depleted, either through microbial respiration or chemical scavenging, the change in SIP response was significantly reduced. This suggests that microbial activity influences SIP response only indirectly—by modulating redox conditions through oxygen depletion.

Control experiments with solder and with epoxy-sealed iron further supported the hypothesis that trace levels of oxygen would be sufficient to produce measurable SIP responses via surface oxidation, even in materials that are less reactive.

These experimental findings were supported by numerical simulations incorporating redox-modified boundary conditions on the surface of metal. Our numerical simulations of SIP response due to iron oxidation successfully reproduced key experimental trends, including the evolution of peak phase shift, peak frequency, and absolute conductivity. By fitting model parameters to the experimental data, we found that surface capacitance (C_0) increased over time, consistent with progressive alteration of the iron

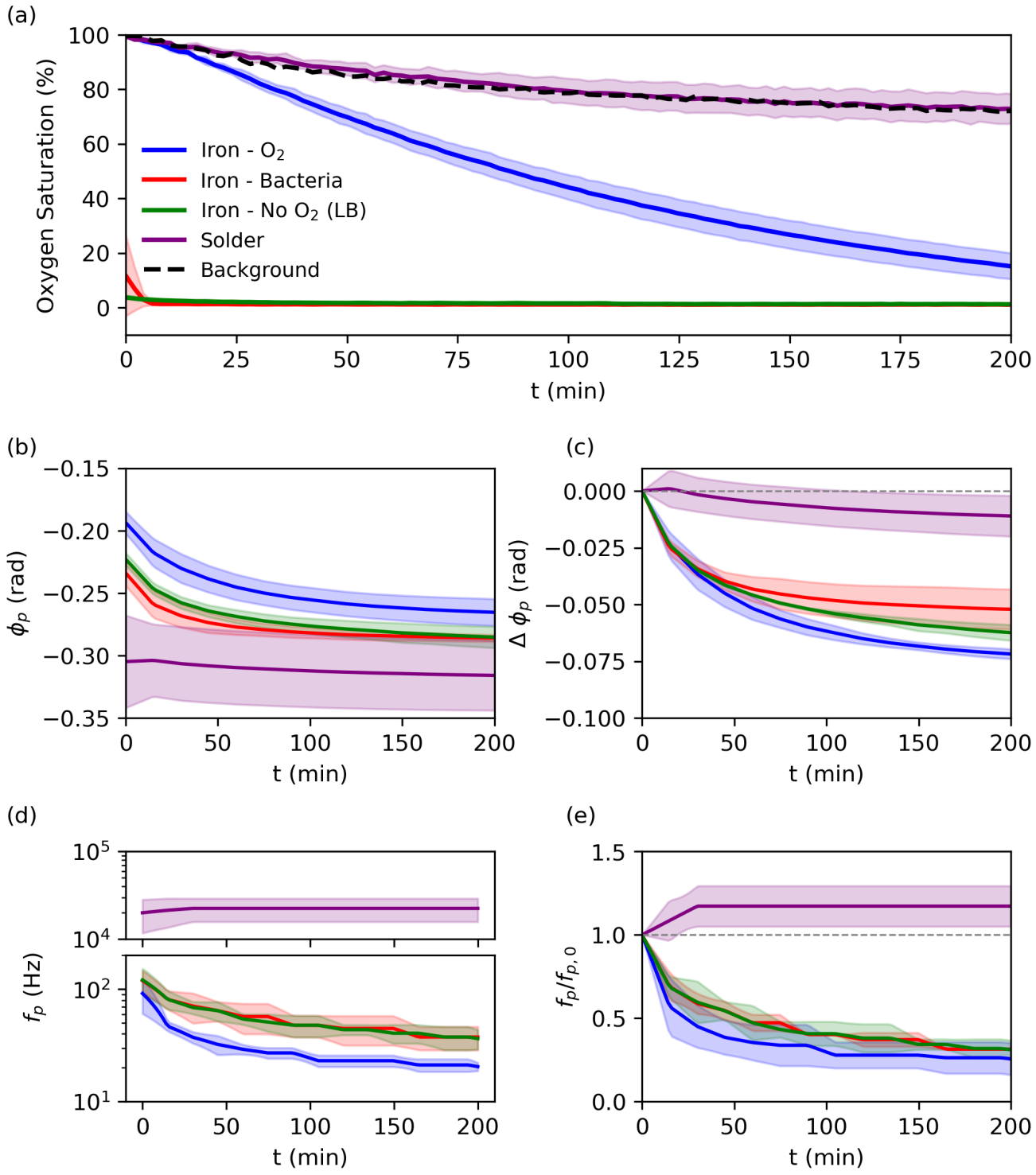


Figure 8. Experimental results from the oxygen consumption experiments. Shaded areas represent one standard deviation from the mean of replicate measurements. (a) Oxygen concentration over time, where 100% corresponds to atmospheric saturation. (b) Temporal evolution of the peak phase shift (ϕ_p). (c) Change in maximum phase shift ($\Delta\phi_p$) relative to the initial value at time zero. (b) Temporal evolution of the peak phase frequency (f_p). (e) Ratio of peak frequency at time t to that at time zero ($f_p/f_{p,0}$).

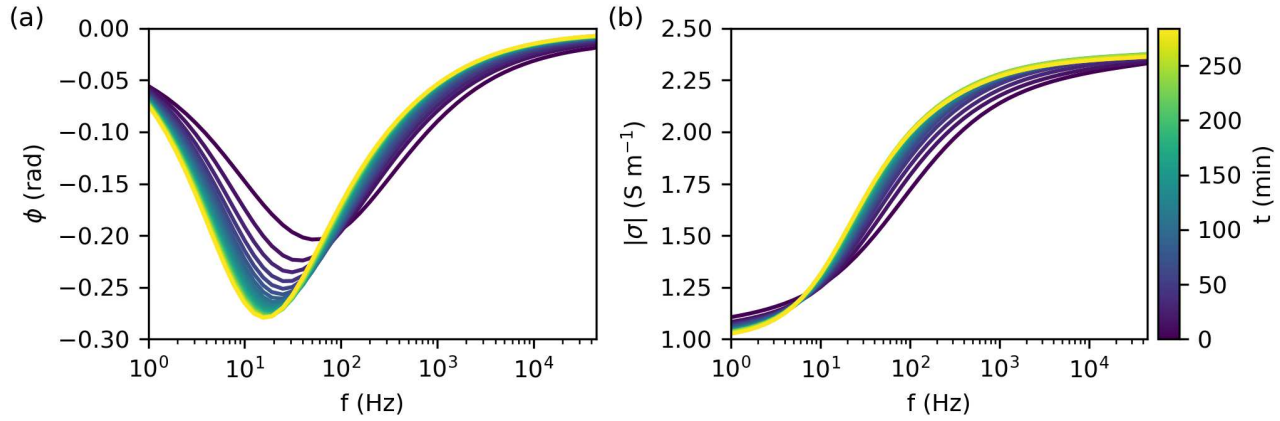


Figure 9. Example results of SIP measurements over time under the iron-with-oxygen condition. (a) Phase shift (ϕ) as a function of frequency at different time points. (b) Absolute conductivity ($|\sigma|$) as a function of frequency at the same time points.

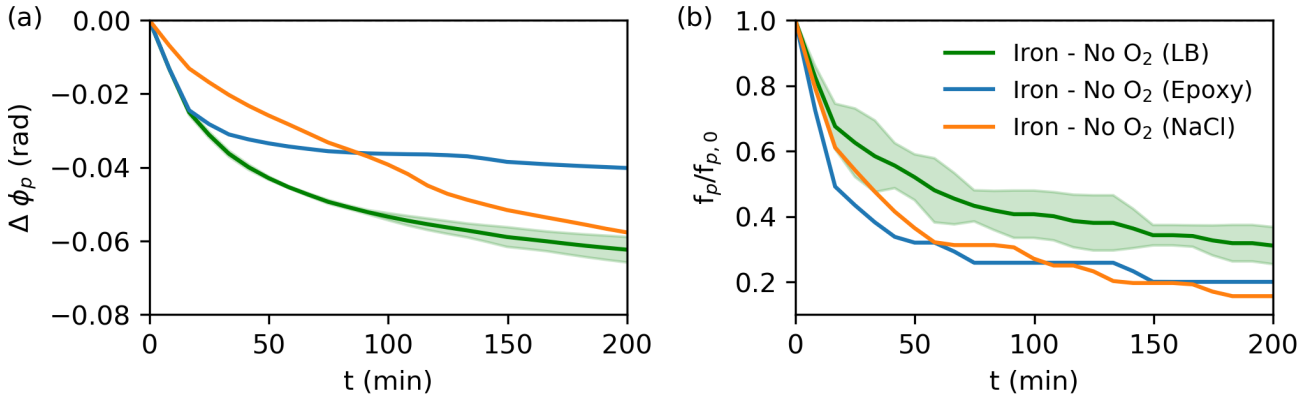


Figure 10. SIP response of iron under oxygen-depleted conditions. Conditions include LB medium with oxygen scavenger (Iron - No O_2 (LB)), LB medium with epoxy-sealed iron ends (Iron - No O_2 (Epoxy)), and NaCl solution with oxygen scavenger (Iron - No O_2 (NaCl)). The shaded region for the LB medium condition represents one standard deviation across replicates. (a) Change in maximum phase shift ($\Delta\phi$) relative to the initial value at time zero. (b) Ratio of peak frequency at time t to that at time zero ($f_p/f_{p,0}$).

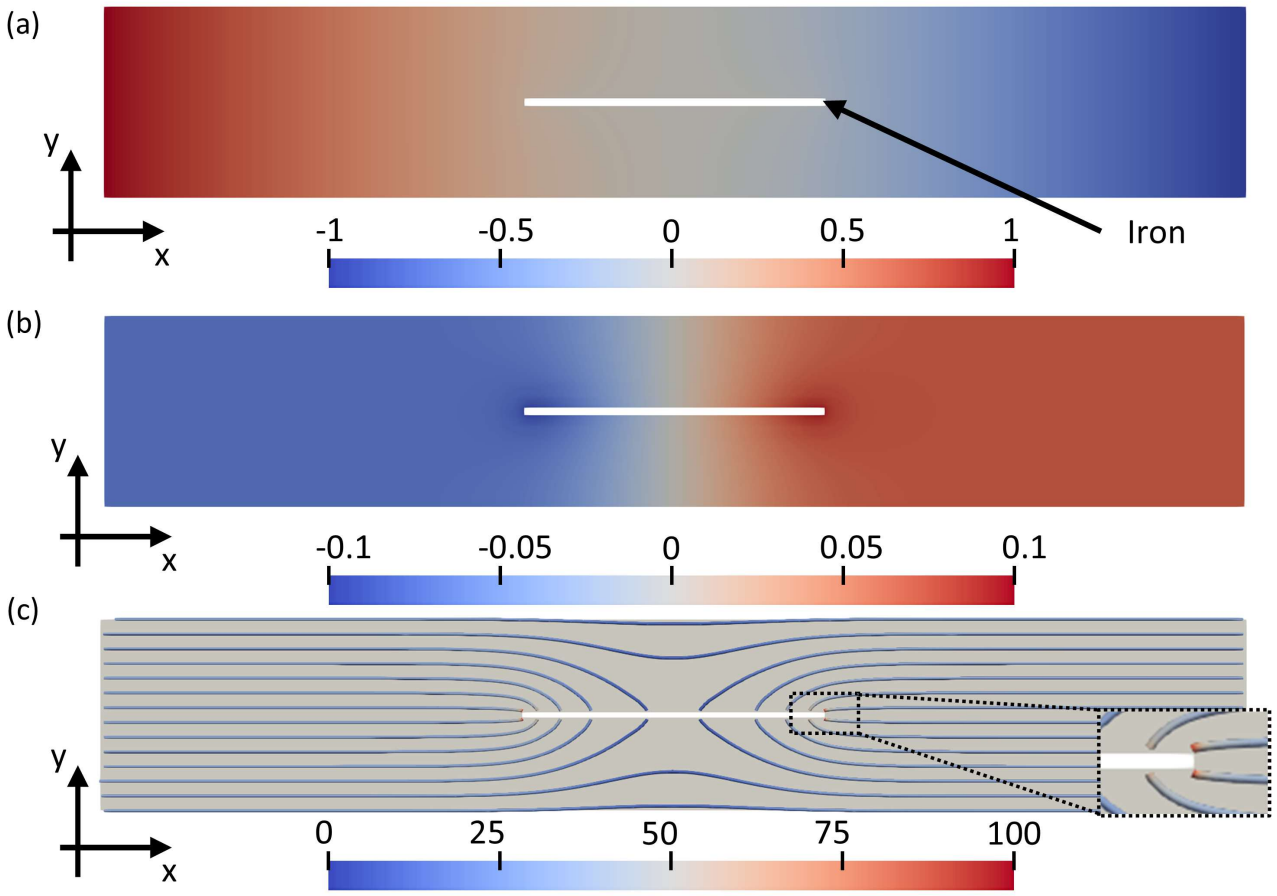


Figure 11. Example simulation results at the peak frequency with parameters $C_0 = 4.8$ and $\alpha = 100\ \mathrm{S\,m^{-2}}$. (a) Real part of the electrical potential. (b) Imaginary part of the electrical potential. (c) Streamlines of the real part of the electrical current. The color scale indicates the magnitude of the current density.

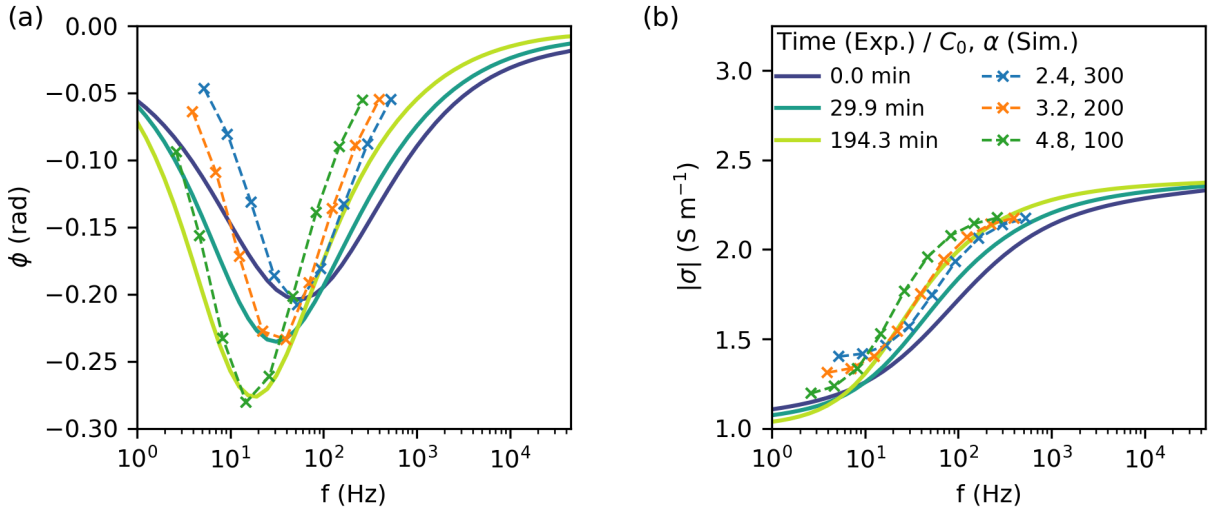


Figure 12. Comparison between selected experimental results (Iron - O_2 condition) and corresponding simulation outputs. (a) Phase shift (ϕ) as a function of frequency. (b) Absolute conductivity ($|\sigma|$) as a function of frequency.

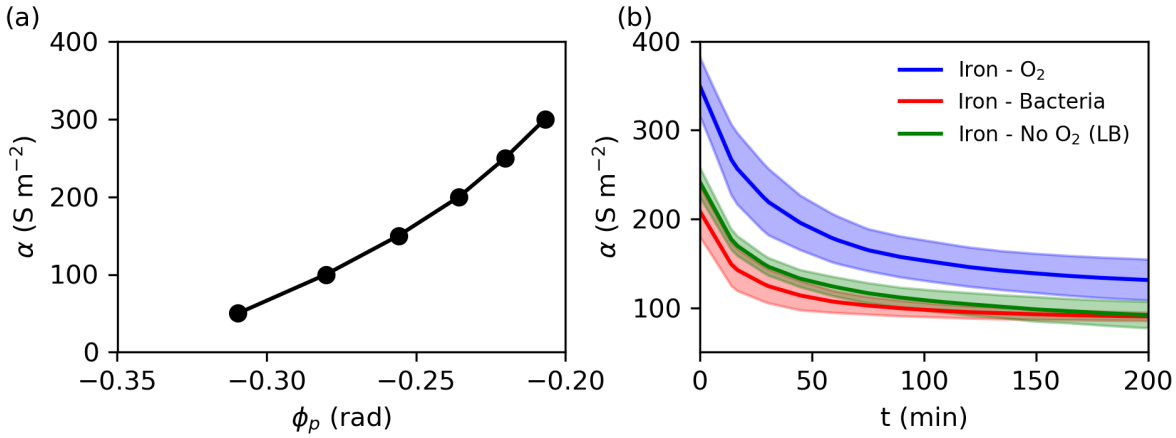


Figure 13. (a) Simulated relationship between peak phase shift (ϕ_p) and redox-driven electron transfer (α). (b) Estimated values of α over time, obtained by fitting the experimental ϕ_p to the simulation results shown in (a).

surface. The electron transfer associated with redox reaction (α) decreased over time, reflecting declining oxidation rates. These estimated α values also confirmed the relative impact of different experimental conditions: oxidation was most pronounced in the presence of oxygen, while it was significantly lower-but still present-in both the iron-with-bacteria and iron-without-oxygen conditions. Notably, even at later stages of the experiment, a nonzero α was required to match observations, supporting the conclusion that trace levels of oxygen are sufficient to sustain surface oxidation and drive measurable SIP responses.

Taken together, our results suggest that microbial activity can influence SIP signals, but only through indirect geochemical effects—most notably, by affecting the redox environment. This distinction is critical for interpreting SIP measurements in environmental and subsurface studies. Apparent correlations between SIP anomalies and microbial activity may not reflect direct microbial polarization, but instead result from microbially driven changes in geochemistry in the presence of other sources of SIP response.

Future work should explore more complex biological processes and mineral interactions under controlled redox gradients to further refine the interpretability of SIP measurements in natural settings.

4 Data Availability

The datasets generated during and/or analysed during the current study are available from the corresponding author on reasonable request.

References

1. Chemla, Y. *et al.* Hyperspectral reporters for long-distance and wide-area detection of gene expression in living bacteria. *Nat. Biotechnol.* 15–21, DOI: 10.1038/s41587-025-02622-y (2025).
2. Kemna, A. *et al.* An overview of the spectral induced polarization method for near-surface applications. *Near Surf. Geophys.* **10**, 453–468, DOI: 10.3997/1873-0604.2012027 (2012).
3. Kessouri, P. *et al.* Induced polarization applied to biogeophysics: recent advances and future prospects. *Near Surf. Geophys.* **17**, 595–621, DOI: 10.1002/nsg.12072 (2019).
4. Abdel Aal, G. Z., Atekwana, E. A. E. A., Slater, L. D. & Atekwana, E. A. E. A. Effects of microbial processes on electrolytic and interfacial electrical properties of unconsolidated sediments. *Geophys. Res. Lett.* **31**, L12505, DOI: 10.1029/2004GL020030 (2004).
5. Williams, K. H. *et al.* Geophysical imaging of stimulated microbial biomineralization. *Environ. Sci. Technol.* **39**, 7592–7600, DOI: 10.1021/es0504035 (2005).
6. Ntarlagiannis, D., Williams, K. H., Slater, L. & Hubbard, S. Low-frequency electrical response to microbial induced sulfide precipitation. *J. Geophys. Res. Biogeosciences* **110**, G02009, DOI: 10.1029/2005JG000024 (2005).
7. Slater, L., Ntarlagiannis, D., Personna, Y. R. & Hubbard, S. Pore-scale spectral induced polarization signatures associated with FeS biomineral transformations. *Geophys. Res. Lett.* **34**, L21404, DOI: 10.1029/2007GL031840 (2007).

8. Personna, Y. R. *et al.* Spectral induced polarization and electrodic potential monitoring of microbially mediated iron sulfide transformations. *J. Geophys. Res. Biogeosciences* **113**, 1–13, DOI: 10.1029/2007JG000614 (2008).

9. Saneiyan, S., Ntarlagiannis, D. & Colwell, F. Complex conductivity signatures of microbial induced calcite precipitation, field and laboratory scales. *Geophys. J. Int.* 51–87, DOI: 10.1093/gji/ggaa510 (2020).

10. Davis, C. A. *et al.* Microbial growth and biofilm formation in geologic media is detected with complex conductivity measurements. *Geophys. Res. Lett.* **33**, n/a–n/a, DOI: 10.1029/2006GL027312 (2006).

11. Ntarlagiannis, D. & Ferguson, A. SIP response of artificial biofilm. *Geophysics* **74**, A1–A5, DOI: 10.1190/1.3031514 (2009).

12. Albrecht, R., Gourry, J. C., Simonnot, M.-O. & Leyval, C. Complex conductivity response to microbial growth and biofilm formation on phenanthrene spiked medium. *J. Appl. Geophys.* **75**, 558–564, DOI: 10.1016/j.jappgeo.2011.09.001 (2011).

13. Abdel Aal, G. Z., Atekwana, E. A., Rossbach, S. & Werkema, D. D. Sensitivity of geoelectrical measurements to the presence of bacteria in porous media. *J. Geophys. Res.* **115**, 1–11, DOI: 10.1029/2009JG001279 (2010).

14. Wu, Y., Surasani, V. K., Li, L. & Hubbard, S. S. Geophysical monitoring and reactive transport simulations of bioclogging processes induced by Leuconostoc mesenteroides. *GEOPHYSICS* **79**, E61–E73, DOI: 10.1190/geo2013-0121.1 (2014).

15. Abdel Aal, G. Z., Slater, L. D. & Atekwana, E. A. Induced-polarization measurements on unconsolidated sediments from a site of active hydrocarbon biodegradation. *Geophysics* **71**, H13–H24 (2006).

16. Mewafy, F. M. *et al.* Evidence that bio-metallic mineral precipitation enhances the complex conductivity response at a hydrocarbon contaminated site. *J. Appl. Geophys.* **98**, 113–123, DOI: 10.1016/j.jappgeo.2013.08.011 (2013).

17. Personna, Y. R., Slater, L., Ntarlagiannis, D., Werkema, D. & Szabo, Z. Complex resistivity signatures of ethanol biodegradation in porous media. *J. Contaminant Hydrol.* **153**, 37–50, DOI: 10.1016/j.jconhyd.2013.07.005 (2013).

18. Atekwana, E. A. & Abdel Aal, G. Z. Iron biomineralization controls on geophysical signatures of hydrocarbon contaminated sediments. *J. Earth Sci.* **26**, 835–843, DOI: 10.1007/s12583-015-0611-2 (2015).

19. Noel, C. *et al.* Suitable real-time monitoring of the aerobic biodegradation of toluene in contaminated sand by spectral induced polarization measurements and CO2 analyses. *Near Surf. Geophys.* **14**, 263–273, DOI: 10.3997/1873-0604.2016007 (2016).

20. Abdel Aal, G., Atekwana, E., Radzikowski, S. & Rossbach, S. Effect of bacterial adsorption on low frequency electrical properties of clean quartz sands and iron-oxide coated sands. *Geophys. Res. Lett.* **36**, 1–5, DOI: 10.1029/2008GL036196 (2009).

21. Zhang, C., Ntarlagiannis, D., Slater, L. & Doherty, R. Monitoring microbial sulfate reduction in porous media using multipurpose electrodes. *J. Geophys. Res.* **115**, 1–11, DOI: 10.1029/2009JG001157 (2010).

22. Strobel, C., Abramov, S., Huisman, J. A., Cirpka, O. A. & Mellage, A. Spectral Induced Polarization (SIP) of Denitrification-Driven Microbial Activity in Column Experiments Packed With Calcareous Aquifer Sediments. *J. Geophys. Res. Biogeosciences* **128**, DOI: 10.1029/2022JG007190 (2023).

23. Mellage, A. *et al.* Linking Spectral Induced Polarization (SIP) and Subsurface Microbial Processes: Results from Sand Column Incubation Experiments. *Environ. Sci. & Technol.* **52**, 2081–2090, DOI: 10.1021/acs.est.7b04420 (2018).

24. Doherty, R. *et al.* A microbial fuel cell in contaminated ground delineated by electrical self-potential and normalized induced polarization data. *J. Geophys. Res. Biogeosciences* **115**, 1–11, DOI: 10.1029/2009JG001131 (2010).

25. Flores Orozco, A. *et al.* Delineation of subsurface hydrocarbon contamination at a former hydrogenation plant using spectral induced polarization imaging. *J. Contaminant Hydrol.* **136-137**, 131–144, DOI: 10.1016/j.jconhyd.2012.06.001 (2012).

26. Chen, J., Hubbard, S. S. & Williams, K. H. Data-driven approach to identify field-scale biogeochemical transitions using geochemical and geophysical data and hidden Markov models : Development and application at a uranium-contaminated aquifer. *Water Resour. Res.* **49**, 6412–6424, DOI: 10.1002/wrcr.20524 (2013).

27. Wainwright, H. M. *et al.* Hierarchical Bayesian method for mapping biogeochemical hot spots using induced polarization imaging. *Water Resour. Res.* **52**, 533–551, DOI: 10.1002/2015WR017763 (2016).

28. Flores-Orozco, A., Gallistl, J., Steiner, M., Brandstätter, C. & Fellner, J. Mapping biogeochemically active zones in landfills with induced polarization imaging: The Heferlbach landfill. *Waste Manag.* **107**, 121–132, DOI: 10.1016/j.wasman.2020.04.001 (2020).

29. Williams, K. H. *et al.* Geophysical Monitoring of Coupled Microbial and Geochemical Processes During Stimulated Subsurface Bioremediation. *Environ. Sci. & Technol.* **43**, 6717–6723, DOI: 10.1021/es900855j (2009).

30. Saneiyan, S. *et al.* Induced polarization as a monitoring tool for in-situ microbial induced carbonate precipitation (MICP) processes. *Ecol. Eng.* **127**, 36–47, DOI: 10.1016/j.ecoleng.2018.11.010 (2019).

31. Izumoto, S. *et al.* Pore-Scale Mechanisms for Spectral Induced Polarization of Calcite Precipitation Inferred from Geo-Electrical Millifluidics. *Environ. Sci. & Technol.* **56**, 4998–5008, DOI: 10.1021/acs.est.1c07742 (2022).

32. Li, Q., Feng, L., Cameron, S. D., Deckman, H. W. & Ertaş, D. Quantifying the origin of membrane polarization. *Geophys. J. Int.* **227**, 1004–1011, DOI: 10.1093/gji/ggab209 (2021).

33. Revil, A., Atekwana, E., Zhang, C., Jardani, A. & Smith, S. A new model for the spectral induced polarization signature of bacterial growth in porous media. *Water Resour. Res.* **48**, W09545, DOI: 10.1029/2012WR011965 (2012).

34. Zhang, C., Revil, A., Fujita, Y., Munakata-marr, J. & Redden, G. Quadrature conductivity: A quantitative indicator of bacterial abundance in porous media. *Geophysics* **79**, D363–D375 (2014).

35. Pilawski, T. *On the impact of bacteria on spectral induced polarization measurements*. Ph.D. thesis, Université de Liège (2019).

36. Zimmermann, E. *et al.* A high-accuracy impedance spectrometer for measuring sediments with low polarizability. *Meas. Sci. Technol.* **19**, 1–9, DOI: 10.1088/0957-0233/19/10/105603 (2008).

37. Silva-Rocha, R. *et al.* The Standard European Vector Architecture (SEVA): a coherent platform for the analysis and deployment of complex prokaryotic phenotypes. *Nucleic Acids Res.* **41**, D666–D675, DOI: 10.1093/nar/gks1119 (2013).

38. Feng, L. *et al.* Quantifying Induced Polarization of Conductive Inclusions in Porous Media and Implications for Geophysical Measurements. *Sci. Reports* **10**, 7–11, DOI: 10.1038/s41598-020-58390-z (2020).

39. Izumoto, S. Induced Polarization of Metal Grains: Simulations of Three-Dimensional Electric Fields. *J. Geophys. Res. Solid Earth* **128**, DOI: 10.1029/2023JB026757 (2023).

40. Izumoto, S. & Nguyen, F. Theory and simulation for low-frequency interfacial polarization of plant root cell. *Geophys. J. Int.* **241**, 1632–1647, DOI: 10.1093/gji/ggaf110 (2025).

41. Hubbard, C. G., West, L. J., Odriguez-Blanco, J. D. & Shaw, S. Laboratory study of spectral induced polarization responses of magnetite-Fe2+ redox reactions in porous media. *Geophysics* **79**, D21–D30 (2014).

42. Wong, J. An electrochemical model of the induced-polarization phenomenon in disseminated sulfide ores. *GEOPHYSICS* **44**, 1245–1265, DOI: 10.1190/1.1441005 (1979).

43. Bücker, M., Flores Orozco, A., Undorf, S. & Kemna, A. On the Role of Stern- and Diffuse-Layer Polarization Mechanisms in Porous Media. *J. Geophys. Res. Solid Earth* **124**, 5656–5677, DOI: 10.1029/2019JB017679 (2019).

Funding

Funding for this research was provided by F.R.S.-FNRS Postdoctoral Fellowship in Belgium (grant No. FC 47069).

Author contributions statement

S.I. planned and performed the experiments, analyzed the results, conducted the numerical simulations, and wrote the manuscript. F.D. planned the experiments and supervised the microbiological aspects, and F.N. planned the experiments and supervised the geophysical aspects. All authors reviewed the manuscript.

Additional information

Competing interests: The authors declare no competing interests.